# Use of forecasting signatures to help distinguish periodicity, randomness, and chaos in ripples and other spatial patterns

David M. Rubin
*U.S. Geological Survey, Menlo Park, California 94025*

(Received 11 May 1992; accepted for publication 21 September 1992)

Forecasting of one-dimensional time series previously has been used to help distinguish periodicity, chaos, and noise. This paper presents two-dimensional generalizations for making such distinctions for spatial patterns. The techniques are evaluated using synthetic spatial patterns and then are applied to a natural example: ripples formed in sand by blowing wind. Tests with the synthetic patterns demonstrate that the forecasting techniques can be applied to two-dimensional spatial patterns, with the same utility and limitations as when applied to one-dimensional time series. One limitation is that some combinations of periodicity and randomness exhibit forecasting signatures that mimic those of chaos. For example, sine waves distorted with correlated phase noise have forecasting errors that increase with forecasting distance, errors that are minimized using nonlinear models at moderate embedding dimensions, and forecasting properties that differ significantly between the original and surrogates. Ripples formed in sand by flowing air or water typically vary in geometry from one to another, even when formed in a flow that is uniform on a large scale; each ripple modifies the local flow or sand-transport field, thereby influencing the geometry of the next ripple downcurrent. Spatial forecasting was used to evaluate the hypothesis that such a deterministic process—rather than randomness or quasiperiodicity—is responsible for the variation between successive ripples. This hypothesis is supported by a forecasting error that increases with forecasting distance, a greater accuracy of nonlinear relative to linear models, and significant differences between forecasts made with the original ripples and those made with surrogate patterns. Forecasting signatures cannot be used to distinguish ripple geometry from sine waves with correlated phase noise, but this kind of structure can be ruled out by two geometric properties of the ripples: Successive ripples are highly correlated in wavelength, and ripple crests display dislocations such as branchings and mergers.

## I. INTRODUCTION

Two-dimensional chaotic (nonperiodic, deterministic) patterns have been created with experiments in fluids,[1,2] video feedback,[3] and computers,[4–6] but the analysis of naturally occurring spatial patterns has lagged behind the analysis of one-dimensional time series. The procedures presented here for forecasting spatial patterns are two-dimensional generalizations of several techniques that recently have been developed for forecasting one-dimensional time series.[7–13] The purpose of this paper is to evaluate the capabilities of two-dimensional forecasting using a variety of synthetic images and then apply those techniques to natural sand ripples formed by wind.

The underlying principle of the time-series forecasting is to predict future behavior for any initial state by consulting a catalog of how the system evolved at other times when initial conditions were similar. Utility of this technique is based on implicit assumptions that the system is stationary and recurrent to arbitrarily close conditions. Predictions are made by selecting a predictee with a known history and known future behavior, searching the catalog for one or more events where the recent time-history approximates the time-history of the predictee, and then using the future behavior of these nearest neighbors in the catalog to predict the future behavior of the predictee. For some purposes—such as weather forecasting, financial forecasting, or noise reduction—determining future behavior is the primary goal of the forecasting. In contrast, for the purpose of characterizing system dynamics, predictions are made primarily to quantify prediction errors as a function of prediction distance,[8,9] embedding dimension, or the number of nearest neighbors used to make the predictions.[10] This predictive process can be thought of as a technique for evaluating the extent to which initial conditions determine future states of the system. System dynamics can also be characterized by comparing forecasts with those made from surrogate data sets that mimic some—but not all—properties of the original time series.[12,13] Eventually it may become possible to use time series or spatial patterns to construct rules or equations that describe system dynamics.[14–16]

## II. FORECASTING PROCEDURE

To forecast a one-dimensional time series of a variable $(x)$,[8–10] the series is split in half. One half is used as a catalog or fitting set to relate the recent history of the system to future states. The other half of the time series (testing set) is used to test the predictive ability of the catalog. At any time $(t)$, the history of the system for $m$ steps through time can be represented by a single point in

 1054-1500/92/040525-11$001.00 © 1992 American Institute of Physics 

Downloaded 28 Apr 2005 to 192.58.150.41. Redistribution subject to AIP license or copyright, see http://chaos.aip.org/chaos/copyright.jsp

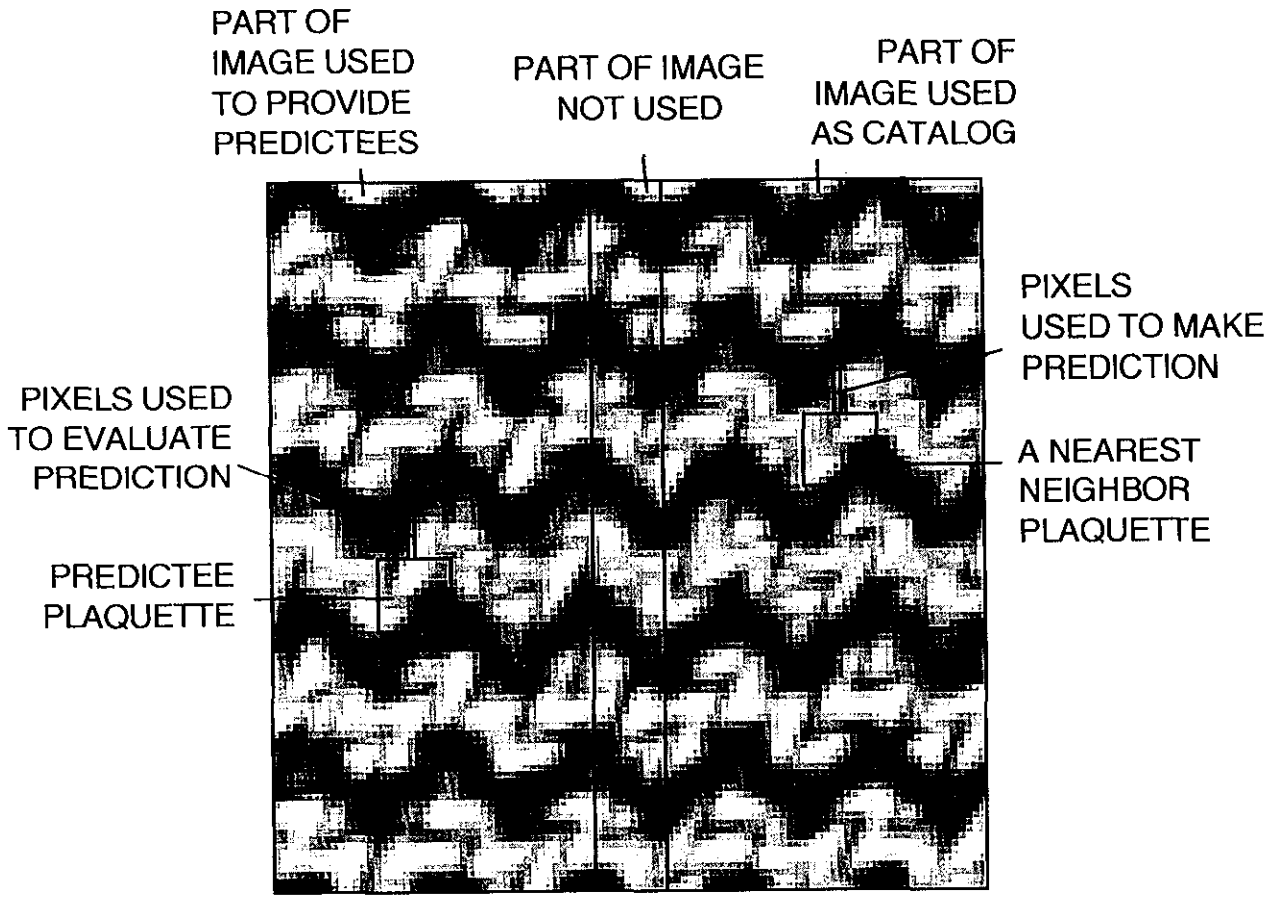


FIG. 1. Diagrammatic representation of the forecasting procedure. An image is divided into two parts, one part for use as a catalog and one part to test predictions. A small area between these two regions is not used in either set, to avoid lateral correlation. The image in this example is 100 pixels square; predictee plaquettes are 10 pixels square, corresponding to an embedding dimension of 100. Each predictee plaquette is compared with all 10-by-10 plaquettes in the catalog, and nearest neighbors are evaluated by the least-squared differences of corresponding pixels in the predictee and catalog plaquettes. The pixels in a strip adjacent to the nearest neighbors in the catalog are used to predict the values of a corresponding strip of pixels adjacent to the predictee. Forecasts can be made using either a local mean value model or a local linear AR model, for a variable number of nearest neighbors (ranging from the single nearest neighbor to the entire set of plaquettes in the catalog). Forecasting errors are measured by comparing the predicted values with the actual values adjacent to the predictee; errors are expressed either as a correlation coefficient between predicted and observed values (Ref. 9) or as the rms error normalized to the standard deviation of the data (Ref. 10). The predictive process is illustrated using a two-dimensional image, but the procedure is computationally identical to representing each plaquette as a point in 100-dimensional space, finding nearest neighbors in this space, and making predictions by tracking the trajectories of those points to their future locations. The image being forecast is a gray-scale image of a quasiperiodic pattern created by superimposing 3 trains of sine waves having differing orientations, wavelengths, and planform sinuosities; values of pixels range from zero (white) to 255 (black).

$m$-dimensional space; the coordinates of that point are given by $(x_t, x_{t-1}, x_{t-2}, \ldots, x_{t+1-m})$. A prediction is made by placing the predictee in this $m$-dimensional space, locating $m$ or more nearest neighbors, and then using least squares to solve

$$x_{t+1} \approx \alpha_0 + \sum_{i=1}^{m} \alpha_i x_{t+1-i} \tag{1}$$

for the coefficients that best relate $x_{t+1}$ to $x_t, x_{t-1}, x_{t-2}, \ldots, x_{t+1-m}$ in the catalog (fitting set). These values for the coefficients are used to predict $x_{t+1}$ for the testing set. The predicted value is then compared with the actual value in the testing set, and predictability is quantified either by the rms error of the predictions[8] or by the correlation coefficient between predicted and observed values.[9] Alternatively, predictions could be computed using the simplex method.[9]

The procedure for forecasting two-dimensional spatial patterns is analogous to the procedure for time series. A digital image is divided in half; one half is reserved as a catalog, and the other is used to provide predictee plaquettes and evaluate predictions (Fig. 1). Each predictee plaquette (and every plaquette with similar size and shape in the catalog) can be represented by a single point in space, where the total number of dimensions is equal to the number of pixels in the plaquette, and the location in each dimension is defined by the intensity of a corresponding pixel. The number of dimensions is equal to the length ($m$) of the plaquette measured in the direction toward which the forecast is being made multiplied by the width ($n$) of



Downloaded 28 Apr 2005 to 192.58.150.41. Redistribution subject to AIP license or copyright, see http://chaos.aip.org/chaos/copyright.jsp

the plaquette in the orthogonal direction. Locating nearest neighbors requires searching the $mn$-dimensional space to find the catalog points closest to a predictee; this is computationally equivalent to shifting the predictee plaquette through every location in the catalog image and using the sum of the squared differences in pixel intensities to determine which plaquettes are most similar to the predictee. Predictions can be made using either the mean value at the corresponding site for the nearest neighbors in the catalog (local constant value predictions) or using nearest neighbors in the catalog to solve

$$x_{(t+1,u)} \approx \alpha_{(0,0)} + \sum_{i=1}^{m} \sum_{j=1}^{n} \alpha_{(i,j)} x_{(t+1-i,u+j-(1+n)/2)} \tag{2}$$

for the coefficients $\alpha_{(0,0)}$ and $\alpha_{(1,1)}$ through $\alpha_{(m,n)}$ by a least-squares fit. The coefficients evaluated for the nearest neighbors in the catalog are then applied to the predictee plaquette in the testing set to make a local linear AR prediction. Equation (2) describes a prediction made along a vertical column ($u$) that is centered left-to-right with respect to a plaquette having a width ($n$) that is an odd number of pixels.

Prediction error is evaluated as a function of prediction distance,[8,9] embedding dimension, and as a function of the number of nearest neighbors ($k$) used to make the predictions.[10] Variation with distance and embedding dimension quantify the extent to which local structure of a spatial pattern defines the adjacent structure; and variation with the number of neighbors evaluates the relative importance of low-dimensional and high-dimensional (or stochastic) dynamics. An additional technique—comparison with forecasts made from surrogate data—was applied to test the null hypothesis that observed spatial irregularity results from linearly correlated noise, rather than nonlinear dynamics.[12,13]

## III. FORECASTING SIGNATURES OF SYNTHETIC IMAGES

### A. Predictability as a function of distance

Six synthetic images (Figs. 1–6) were created and analyzed: a quasiperiodic pattern, a spatio–temporal chaotic pattern, and four kinds of patterns with random attributes (two-dimensional white and brown noise, random placement of small uniform patterns, and randomly distorted sine waves). In the one-dimensional case, predictability of periodic time series remains high regardless of how far the predictions are projected into the future. Similarly, predictability is high for periodic and quasiperiodic spatial patterns—regardless of prediction distance—provided that the sample area is large enough to contain a good variety of the relative phasing of the individual periodic components (Fig. 7). If the sample plaquette is too small, however, low-frequency information is not included, and predictability decreases and increases with prediction distance in what resembles a beat-frequency process.

The forecasting signature of a chaotic pattern (specifically, a spatio–temporal transient chaotic pattern) is illustrated using a synthetic image (Fig. 2) that was created using the "dripping handrail" model.[4] Each vertical column in the image represents conditions at a different site along a handrail; each horizontal row represents a step

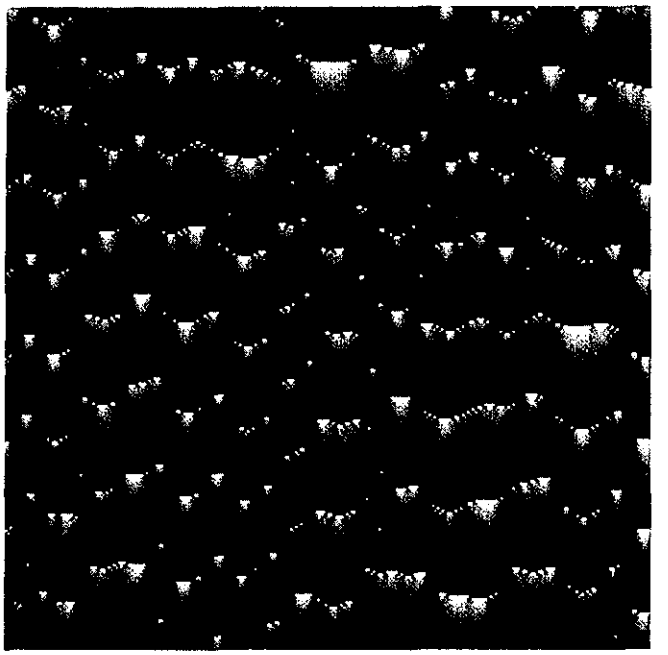

FIG. 2. Spatio–temporal chaotic pattern created using the dripping handrail, coupled-lattice, model of Crutchfield and Kaneko (Ref. 4). Pixel intensity at 256 lattice sites (left to right across the image) represents the thickness of a film of water at 256 steps through time (top to bottom). Mean "wavelength" is approximately 30 pixels.

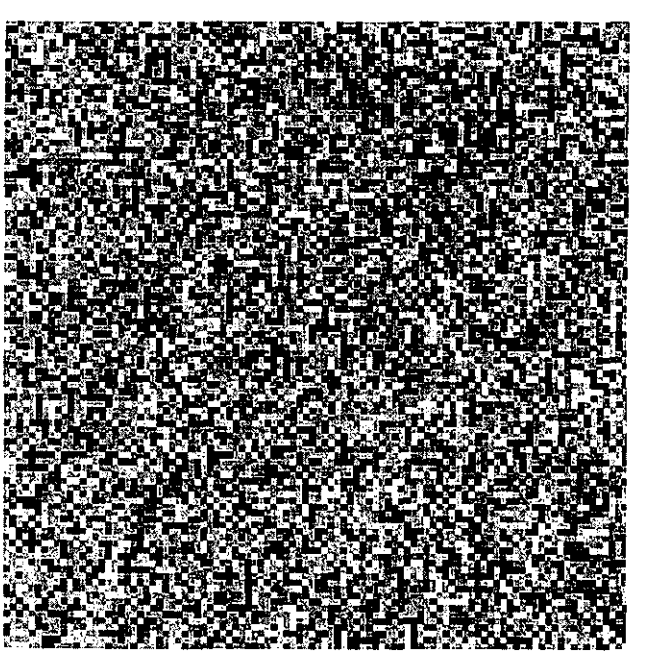

FIG. 3. Speckled pattern created using random numbers to define the intensity of each pixel in a 100-by-100 image. This is an example of two-dimensional white (uncorrelated) noise.



Downloaded 28 Apr 2005 to 192.58.150.41. Redistribution subject to AIP license or copyright, see http://chaos.aip.org/chaos/copyright.jsp

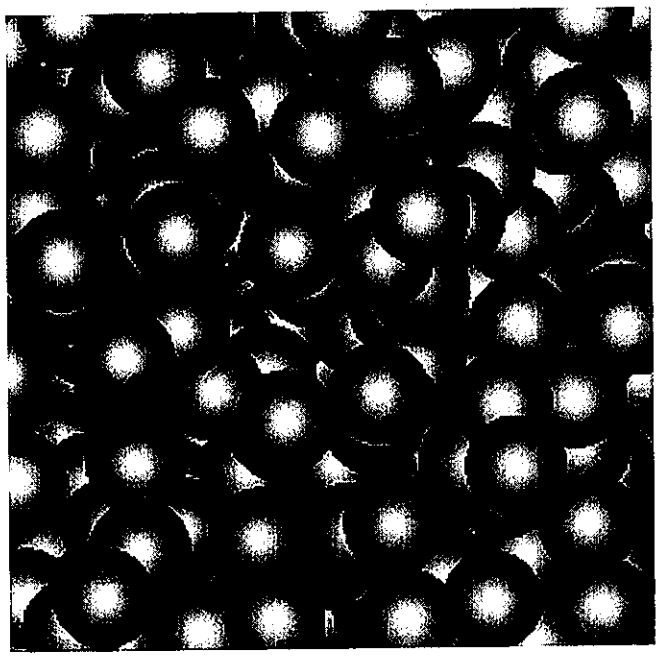

FIG. 4. Image created by repeatedly superimposing circular patterns at random locations. Image is 256 pixels square, and the diameter of each circle is 40 pixels. The structure of each circular area is deterministic, but the location of each circle is not.

through time. Pixel intensity represents the thickness of a film of water on the lower surface of the handrail. At each site, the thickness of the film of water increases through time (top-to-bottom in the image) until surface tension is exceeded at that site, and water drips from the handrail.

FIG. 5. Pattern created by sequentially faulting a plane 2000 times at random locations. The resulting image is a 256 pixel square of two-dimensional $1/f^{\alpha}$ (brown) noise; in this example, $\alpha \approx 2$.

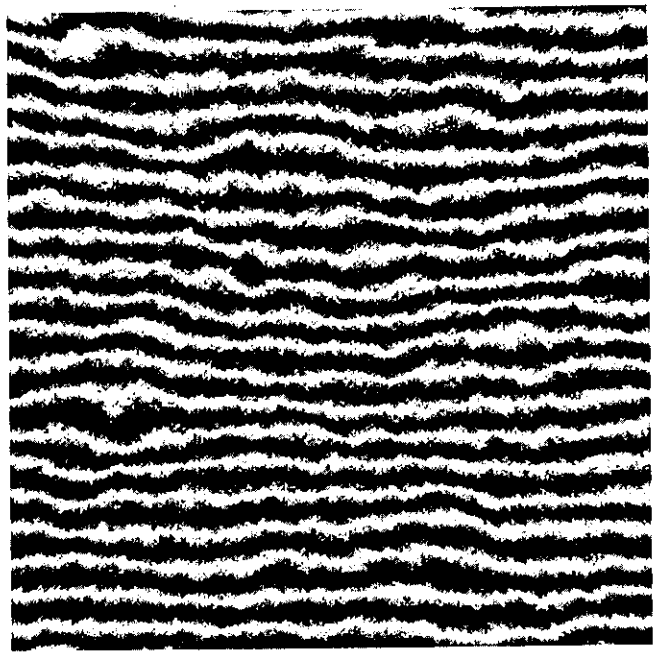

FIG. 6. Pattern created by randomly distorting a field of sine waves with correlated phase noise, as defined by Eq. (3); $\epsilon$ is defined by the corresponding local value in Fig. 5.

Coupling between adjacent sites causes water to flow along the one-dimensional lattice that represents the handrail. These rules produce a chaotic pattern in which the value at any site is a deterministic nonlinear function of the preceding values at that site and at the two adjacent sites, in

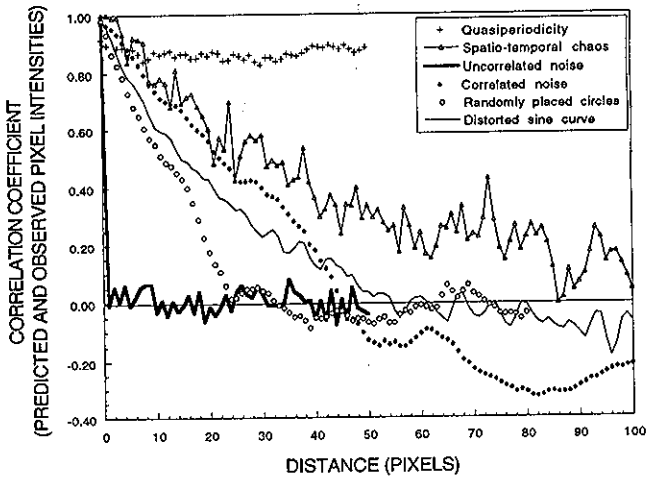


FIG. 7. Plot of predictability (correlation coefficient between predicted and observed pixel intensities) as a function of forecasting distance for the six patterns in Figs. 1–6. Predictions in this plot were based on local constant value models. Plot shows four classes of forecasting behavior: predictability remains at a relatively high, constant, value for all prediction distances (quasiperiodic pattern); predictability drops to zero at a prediction distance of only a single pixel (two-dimensional white noise); predictability is high for short distances but decays to a value of zero over greater distances (spatio–temporal chaos, randomly placed circular patterns, and distorted sine curve); and predictability decreases with distance but does not stabilize at a value of zero (two-dimensional brown noise).


Downloaded 28 Apr 2005 to 192.58.150.41. Redistribution subject to AIP license or copyright, see http://chaos.aip.org/chaos/copyright.jsp

essentially the same manner that each value in a chaotic time series is a function of preceding values. The resulting pattern has a predictability that decays to a stable value of zero (at a larger number of time steps than plotted in Fig. 7). The predictability is high for a distance of several "wavelengths" because of the deterministic structure of the pattern, but the system is unpredictable for large distances.

The simplest kind of random spatial pattern—a speckled white-noise pattern in which the intensity of each pixel is determined by a random number, and the value at each pixel is independent—exhibits a predictability that falls to zero at a prediction distance of only a single pixel (Figs. 3 and 7). The pattern is completely unpredictable because it contains no deterministic structure. Previous work on forecasting one-dimensional time series has considered a combination of a periodic signal and uncorrelated noise. Sugihara and May[9] showed that observational noise reduces the predictability of the system, but the predictability nevertheless remains relatively constant with prediction time.

Unlike the uncorrelated noise evaluated by Sugihara and May, the predictability of correlated noise and some combinations of deterministic and randomness decay with prediction distance, thereby mimicking the property Sugihara and May found for chaotic systems. To identify these kinds of systems requires other tests such as those described in later sections (variation of predictability with number of nearest neighbors or comparison with surrogate data). One such combination of determinism and randomness is a spatial pattern created by random placement of a smaller pattern (for example, concentrically graded circles are randomly placed in Fig. 4). Predictability for this kind of pattern is high for short distances and decays to zero (Fig. 7). The high predictability for short distances results from the deterministic structure of the graded circles. Random placement of these circles, however, causes the predictability to decrease to zero as distances approach or exceed the diameter of the circles. The predictability of such a pattern crudely resembles that of chaotic patterns, but in this case the decay appears nearly linear. Although these results were obtained with two-dimensional images, a decay in predictability also could be expected for one-dimensional time series from systems in which a constant event occurs at random or irregular times.

A different kind of random pattern can be synthesized by repeatedly faulting (uplifting or down-dropping) the two regions of a plane separated by randomly placed lines (Fig. 5), creating patterns that can be thought of as two-dimensional $1/f^{\alpha}$ noise (where $f$ is frequency, and $\alpha$ is a constant; in this example $\alpha \approx 2$). The predictability of such patterns decays with distance, but does not necessarily stabilize at zero (Fig. 7). For example, in the image shown in Fig. 5, systematic low-frequency differences between the testing half and the catalog half of the image cause long-distance predictions to have a negative correlation (predictions are worse than random). This example demonstrates that this kind of forecasting is not appropriate for nonstationary systems.

The final synthetic pattern (Fig. 6) to be considered was defined by

$$y = \sin(x + \epsilon), \tag{3}$$

where $y$ is pixel intensity, $x$ is distance from top to bottom in the image, and $\epsilon$ is the local value in the accompanying image of brown noise (Fig. 5). The resulting pattern contains both deterministic ($x$) and random ($\epsilon$) attributes, and represents a field of sine waves with a correlated phase distortion. Predictability of this pattern decays and stabilizes at zero (Fig. 7), as do forecasts of chaotic patterns.

Comparison of the predictability curves in Fig. 7 illustrates that identifying chaotic systems is more difficult than suggested by Sugihara and May.[9] A variety of systems—including correlated noise or combinations of determinism and randomness—exhibit forecasting errors that increase with distance. The difficult problem of distinguishing such systems from low-dimensional chaos is considered below.

### B. Predictability as a function of number of nearest neighbors

Recently Casdagli[10] described a technique to use the character of forecasting errors to evaluate the relative importance of linear and nonlinear dynamics of a system. This technique measures short-term forecasting error as a function of the number of neighbors ($k$) used to make predictions. At one extreme (stochastic linear autoregressive modeling), the coefficients in Eqs. (1) or (2) are evaluated once for the entire fitting set, and the resulting coefficients are used for all forecasts of the testing set. By maximizing the size of the sample used to evaluate the coefficients, forecasts maximize noise reduction but minimize sensitivity to the specific initial conditions for the event that is being forecast. At the other extreme (nonlinear deterministic modeling) the coefficients in Eqs. (1) or (2) are reevaluated for each forecast, using only a small sample of nearest neighbors in the fitting set. Noise reduction is poorer because the sample is smaller, but sensitivity to initial conditions is improved because the nearest neighbors used to evaluate the coefficients are chosen selectively. At intermediate numbers of nearest neighbors, modeling is both nonlinear and stochastic. Casdagli argued that the dynamics of a system can be characterized by the kind of model that makes the most accurate short-term forecasts. Thus, low-dimensional nonlinear chaotic behavior can be distinguished from high-dimensional or stochastic behavior, depending on which model gives the most accurate forecasts.

This technique was applied to the six spatial patterns shown in Figs. 1–6. As expected, uncorrelated noise, correlated noise, and quasiperiodicity were most accurately described by linear stochastic models (Fig. 8). Determining the relative accuracy of linear and nonlinear models, however, is more complicated than comparing forecasting errors that were evaluated using a single arbitrary embedding dimension and delay time. Computations made using linear time series (sinusoidal series with one or more frequencies and a few percent of added uncorrelated noise) found that nonlinear stochastic models performed better over a wide range of embedding dimensions. In some cases, the advantage of the nonlinear models over linear models



Downloaded 28 Apr 2005 to 192.58.150.41. Redistribution subject to AIP license or copyright, see http://chaos.aip.org/chaos/copyright.jsp

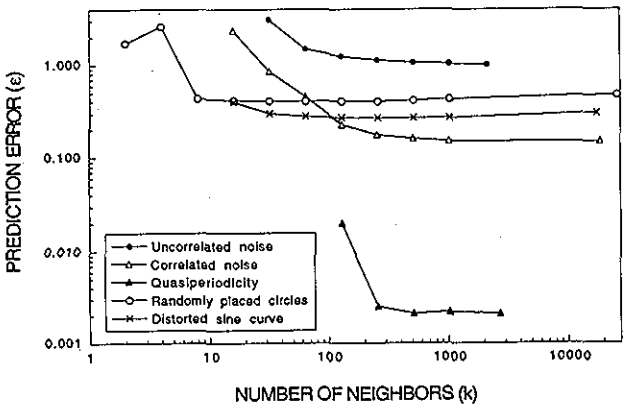


FIG. 8. Forecasting error plotted as a function of the number of nearest neighbors used to make predictions. Local linear forecasts are for distances of 1 pixel. Errors are normalized with respect to the standard deviation of the original image. Forecasts for the quasiperiodic image shown in Fig. 1 are based on plaquettes 10 pixels square, corresponding to an embedding dimension of 100. The total number of neighbors in the catalog ($k_{TOTAL}$) is 1271; number of predictees is 196. An embedding dimension of 100 was found to give better forecasts than smaller values (a factor of 20 better than an embedding dimension of 4 and a factor of 10 better than an embedding dimension of 25); not all plaquette shapes were tested. Forecasts for the uncorrelated noise in Fig. 3 are based on 5 pixel square plaquettes (corresponding to an embedding dimension of 25). The best model is a linear stochastic model that employs the entire catalog ($k_{TOTAL}=2116$; 529 predictees). The model merely predicts the mean value of the image; the rms error is thus equal to the standard deviation of the original image, resulting in a normalized rms error equal to 1. Forecasting errors for the randomly placed circular patterns in Fig. 4 are based on 2 pixel plaquettes. The lowest forecasting errors are for nonlinear stochastic models employing tens or hundreds of nearest neighbors ($k_{TOTAL}=25\,830$; 325 predictees). For the correlated noise shown in Fig. 5, plaquette size is 4 pixels square, but only the 4 corner pixels are evaluated, corresponding to an embedding dimension of 4. The best model is a linear stochastic model employing all neighbors in the catalog ($k_{TOTAL} \doteq 18\,724$; 775 predictees). Forecasts for the distorted sine curve in Fig. 6 are based on plaquettes 5 pixels square (only sampling every other pixel in the two dimensions, corresponding to an embedding dimension of 9; $k_{TOTAL}=17\,365$; 775 predictees). The lowest forecasting errors are for nonlinear stochastic models employing hundreds of nearest neighbors. The advantage of such models over the best linear model that was tested is approximately 11%.

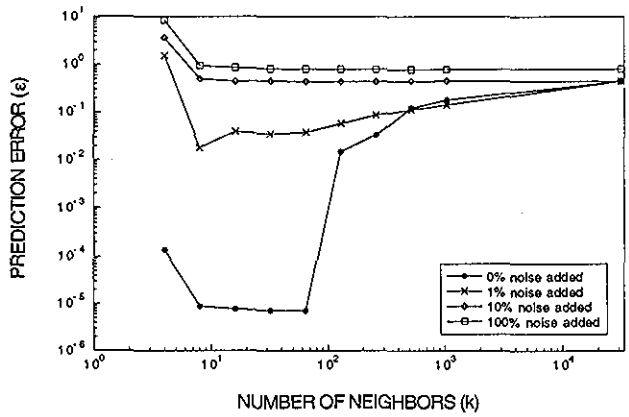


FIG. 9. Forecasting error for the dripping handrail image shown in Fig. 2, with additive uncorrelated noise. Forecasts (208 predictees) are for distances of 1 pixel and are based on plaquettes 3 pixels wide by 1 pixel high, (corresponding to an embedding dimension of 3, the known dynamics of the equations used to create the image). For noise levels of 0% and 1%, the best models are nonlinear, employing few of the 19 656 neighbors in the catalog. For noise levels of 10% and 100%, errors are much greater, and the best models are at the linear stochastic extreme.

exceeded an order of magnitude. For all of these linear series, however, forecasting error could be minimized using linear models with relatively large embedding dimensions; in some cases it was necessary to increase the embedding dimension to nearly 100. At lower embedding dimensions, no models performed as well as the high-dimension linear models, and, moreover, the nonlinear models outperformed linear models.

These results illustrate a possible pitfall of using forecasting error to distinguish linear and nonlinear dynamics. The relative performance of the models depends in part on such modeling parameters as embedding dimension and delay time. The fact that a nonlinear model outperforms a linear model at low embedding dimensions does not demonstrate that the system is nonlinear; the system might be modeled even more accurately using a high-dimension linear model. This demonstrates the importance of attempting forecasts for a range of embedding dimensions and delay times.

In contrast to the uncorrelated noise and sine curves that are best modeled with linear models, the chaotic dripping handrail pattern is most accurately modeled near the deterministic nonlinear extreme (Fig. 9). This chaotic pattern also differs from the linear patterns in that increasing the embedding dimension results in much poorer forecasts. If uncorrelated noise is added to the dripping handrail pattern, forecasting accuracy decreases—particularly for the nonlinear forecasts. Noise levels approaching or exceeding 10% preferentially degrade the nonlinear predictions to such an extent that nonlinear models become less accurate than linear models. Evidently, sensitivity to initial conditions of the nonlinear model has become less an advantage than noise-reducing capability of the linear model.

The most accurate forecasts for the randomly placed circles and distorted sine curve were obtained using nonlinear stochastic models (Fig. 8), but the improvement over linear models is relatively slight (16% and 11%, respectively). The sinusoidal pattern with correlated phase distortion [Fig. 6, as defined in Eq. (3)], is particularly interesting because the combination is more accurately modeled by nonlinear stochastic models, despite the fact that the periodic and random components are individually forecast most accurately using linear models. In this case, the cause of the nonlinearity is not low-dimensional chaos but rather is a sinusoidal transformation of correlated noise; deviation from a linear, periodic, sinusoidal pattern results from randomness. As in the case of the dripping handrail, however, increasing the embedding dimension results in poorer forecasts.

### C. Comparison with surrogate images

Another approach in forecasting has been to compare forecasts of an original time series with forecasts made from surrogate series.[12,13] The surrogates are created to mimic some, but not all, attributes of the original. For



Downloaded 28 Apr 2005 to 192.58.150.41. Redistribution subject to AIP license or copyright, see http://chaos.aip.org/chaos/copyright.jsp

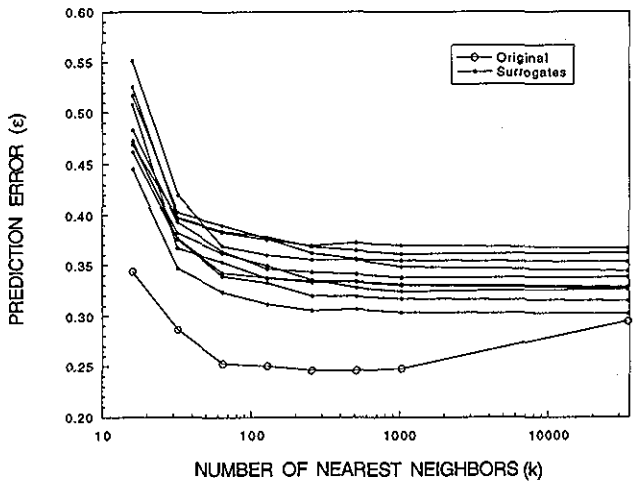


FIG. 10. Forecasting errors for distorted sine waves (Fig. 6) and 10 surrogates. The surrogates have the same power-spectral magnitudes as the original, but have randomized phases. Forecasts (for 250 predictees) are for 1 time step and an embedding dimension of 9. Predictions for the original image are best using nonlinear stochastic models employing several hundred nearest neighbors (out of the 34 364 in the catalog).

example, surrogates made to have the same FFT magnitudes as the original—but having randomized phases—can be used to test the null hypothesis that the original time series is linearly correlated noise. If the original and surrogate time series have significantly different forecastability, then this hypothesis can be rejected.

A two-dimensional analog of this technique was applied to the distorted sine waves with correlated phase noise illustrated in Fig. 6. A two-dimensional FFT was made of the original, the phases were randomized, and surrogate images were created by inverting the FFTs. Forecasts differ between the original and the 10 surrogates (Fig. 10). The surrogates are forecast most accurately using linear models; the original is forecast most accurately by nonlinear models at relatively low embedding dimension, and those forecasts are significantly better than the best models for the surrogates.

These forecasting properties distinguish the original from linearly correlated noise, and lead to the conclusion that the distorted sine pattern contains a nonlinear structure not present in the surrogates. But as noted in the preceding section, the nonlinearity arises from the sinusoidal transformation of correlated noise, not low-dimensional chaos. Although the surrogate technique correctly rejects the null hypothesis, rejecting this particular null hypothesis is insufficient to demonstrate chaos.

## IV. GEOMETRY AND DYNAMICS OF RIPPLES AND DUNES

### A. Background

Virtually all studies of the geometry of bedforms such as ripples and dunes have been directed at determining how mean bedform geometry varies for differing flow conditions. In contrast, the work reported here was undertaken to understand differences in geometry of adjacent bedforms in a train created by a single flow. Hypotheses to explain this variation include quasiperiodicity, randomness, or deterministic chaos resulting from modification of the flow or sand-transport field by the bedform immediately upstream.

Most previous models of ripples and dunes have treated such bedforms as periodic[17,18] or random,[19] but several morphologic and behavioral characteristics suggest that the complexity is self-organized. Even where flow is uniform (when averaged on a scale that is large relative to individual ripples), geometric variation of bedforms is ubiquitous. A deterministic cause for this complexity is suggested by experiments and theoretical models demonstrating that ripples perturb the local boundary layer or sand-transport field, thereby modifying the conditions that shape the next ripple downstream.[20–23] In wind, ballistic grain impacts are believed to be more important than fluid effects, and self-organization has been suggested to arise from a sorting process that causes adjacent ripples to attain similar sizes and migration speeds.[20,21]

In flowing water, this downstream coupling occurs because the local flow near the bed is influenced directly by the bedform immediately upstream. In some flows, placing a single artificial ripple or obstacle on a flat bed can be sufficient to induce formation of a train of ripples downstream,[22,23] even in a flow where ripples otherwise would not form [Fig. 11(a)]. Similar spatial patterns can be simulated using the dripping handrail model starting from initial conditions that are uniform except for a slight perturbation [Fig. 11(b)]. In the model, each horizontal row in the image represents a step through time and is computed from the conditions at the previous time. In the real ripple pattern, each row represents an increasing distance downstream and develops in response to upstream conditions. In both the real and computational examples, the patterns that develop illustrate a similar sensitivity to initial (previous or upstream) conditions.

A complete treatment of ripple dynamics requires an additional dimension of complexity beyond that implied above. The discussion above implies that the downcurrent ripple geometry is a function of upcurrent geometry—unchanging through time. Although this is true for some flows [such as illustrated in Fig. 11(a)], in most flows ripple dynamics is more properly considered as a two-dimensional spatial system that evolves through time as individual ripples interact while migrating downcurrent.

In some ripple fields, down-current coupling produces current-parallel lanes of ripples with abrupt discontinuities between lanes.[24] Such structure implies that across-current coupling of the real ripples is weak relative to downcurrent coupling, an hypothesis that is supported by computational experiments with the dripping handrail model. In addition to these reported spatial variations in individual ripples in uniform flows, both field observations and laboratory experiments have found that the planform geometry of dunes becomes more complex as flow strength increases.[24,25] This increasing spatial complexity is analogous to the increasing complexity observed at increasing flow strengths in couette cylinders[1] and convection cells.[2]


Downloaded 28 Apr 2005 to 192.58.150.41. Redistribution subject to AIP license or copyright, see http://chaos.aip.org/chaos/copyright.jsp

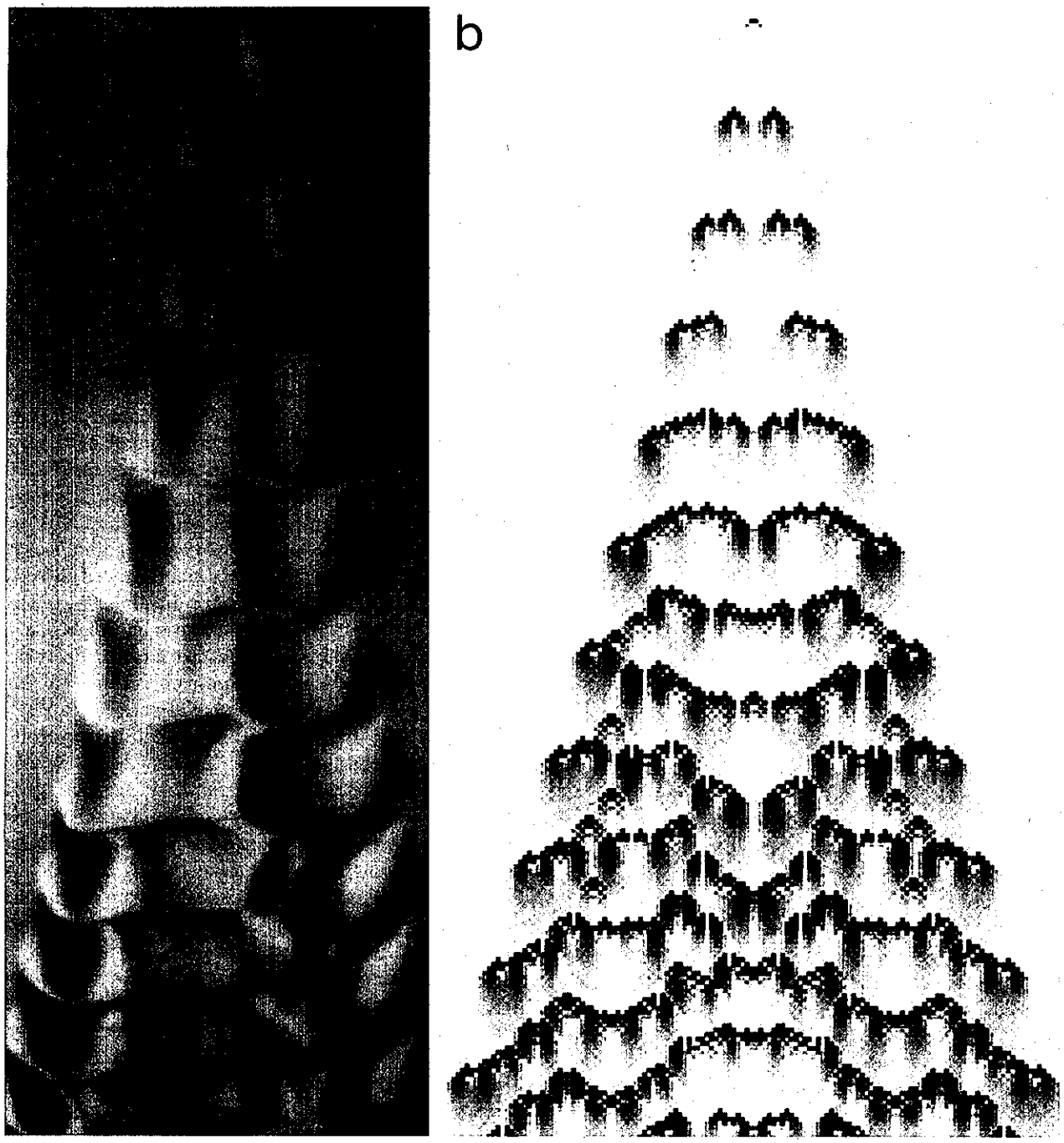


FIG. 11. Development of instabilities beginning from a slight artificial perturbation. (a) Planform view of an experiment to create ripples on a flat bed in flowing water. No sand transport occurred until a mound of sand was placed on the bed. The mound disturbed the flow, producing another bedform, which in turn disturbed the flow, and so on downcurrent (from top to bottom). Photograph from Southard and Dingler (Ref. 23), digitally processed to reduce perspective distortion. (b) Computer simulation of spatial differences using the dripping handrail model, beginning with initial conditions (top of image) that were uniform except for a single pixel. Image is a recomputation of Crutchfield and Kaneko (Ref. 4) (Fig. 45). In both (a) and (b), conditions at the top of the image determine the structure at lower locations.

### B. Forecasting ripple geometry

A photograph of ripples formed by wind (Fig. 12) was digitized and analyzed using the spatial forecasting techniques discussed above; pixel intensity is used to represent ripple geometry. Unlike the synthetic images, in which intensity is proportional to elevation, intensity in the digitized photograph image is more nearly a function of slope.

Predictability of the digitized ripple pattern decays to a value that fluctuates around zero (Fig. 13). As discussed above, such a forecasting signature does not result from white noise or from periodic or quasiperiodic systems, but can result from either chaos or some combinations of periodicity and randomness.

As in the case of one-dimensional time series, forecast-


Downloaded 28 Apr 2005 to 192.58.150.41. Redistribution subject to AIP license or copyright, see http://chaos.aip.org/chaos/copyright.jsp

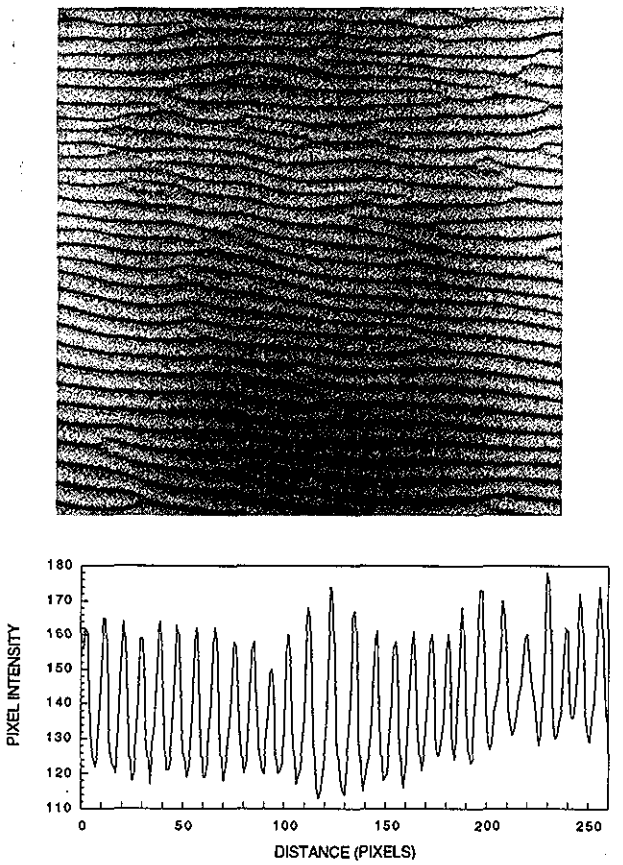


FIG. 12. (a) Photograph of natural ripples formed by wind blowing over a sand bed that is otherwise flat. Wind direction is from top to bottom; ripple wavelength is approximately 10 cm (corresponding to 8.3 pixels after the photograph was digitized). (b) Profile across ripples in (a), showing values of pixels along the left edge of the image, from top to bottom (after digitization).

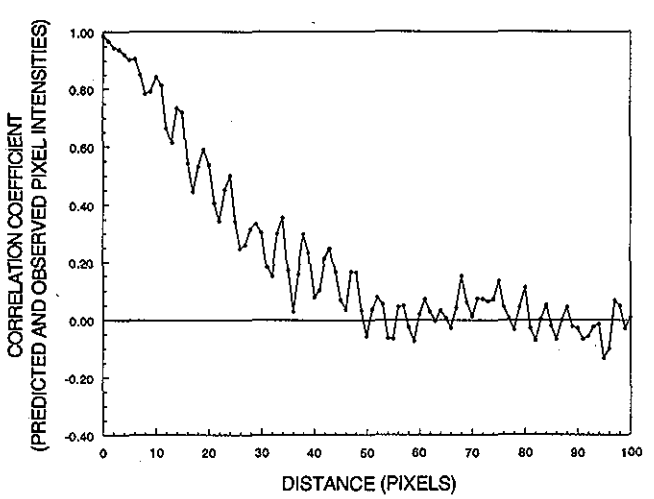


FIG. 13. Predictability of ripples shown in Fig. 12 (a) is initially high but decays to zero by a distance of approximately 60 pixels (7 wavelengths) downwind. This predictability can result from chaos or combinations of periodicity and randomness.

ing errors of spatial patterns depend on embedding dimension (actually two embedding dimensions—an embedding length and an embedding width, corresponding to the number of pixels in the plaquette's downwind and acrosswind directions). The effect of embedding dimension on forecasting error is shown in Fig. 14. The best forecasts are obtained using an embedding length of 9 pixels (slightly greater than the mean wavelength of 8.3 pixels) and a width of 5 pixels. This result is in good agreement with the hypothesis that the geometry of any one ripple depends on the geometry of the ripple immediately upstream.

Forecasting error was also measured as a function of the number of nearest neighbors used to make the predictions—for the original ripples and 11 surrogates (Fig. 15). The model that best predicts the original pattern is a nonlinear stochastic model, which offers a 60% improvement over the best linear model. Forecasting errors for the original image are significantly better than for the surrogates. (The difference is as great as 8 sigmas.[12] That is, the difference between the error for the original and the mean error for the surrogates is 8 times the standard deviation of the errors for the surrogates.) Both of these properties (most accurate predictions with a nonlinear model and significant differences in forecasting error between the real and surrogate pattern) are consistent with the hypothesis that the structure is chaotic, but are also compatible with a field of sine curves with correlated phase distortion.

Differences between the original and surrogate images are visually apparent, as has been noted for original and surrogate time series.[12] Crests and troughs of the surrogate wave forms are relatively discontinuous and irregular in planform, and high-frequency wave forms are visible as separate peaks. These high-frequency wave forms are not visible in the original. Evidently, the phases of these harmonics in the original are related in such a way as to modify the shape of the ripples rather than defining separate smaller ripples.

Visual inspection of the original ripples suggests that variations in ripple geometry are not random, but rather that similar sizes, orientations, and shapes tend to be organized in groups [Figs. 11(a) and 12]. To document one such property of the ripples in Fig. 12, the correlation coefficient was calculated between all successive pairs of ripple wavelengths (measured in a direction normal to the mean crest orientation). The resulting correlation coefficient (0.5) demonstrates that variation between adjacent ripples is at least partially deterministic. In contrast, the structure defined by Eq. (3) has a deterministic mean wavelength, but fluctuations around the mean are uncorrelated. Moreover, crests of the real ripples are disrupted by dislocations (branchings and mergers) that are not present in sine waves distorted by correlated phase noise. Although these geometric properties can be used to reject this particular null hypothesis, it is possible that other more complicated combinations of periodicity and randomness might be formulated to mimic the forecasting signatures, correlated wavelengths, and dislocations of the observed ripples.



Downloaded 28 Apr 2005 to 192.58.150.41. Redistribution subject to AIP license or copyright, see http://chaos.aip.org/chaos/copyright.jsp

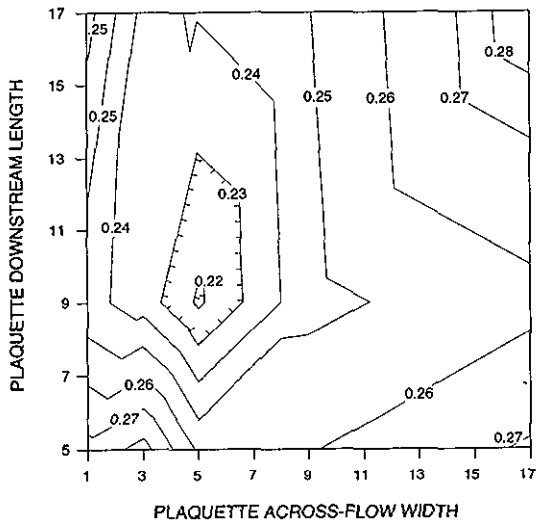


FIG. 14. *Predictability of wind ripples in* Fig. 12 (a) as a function of embedding dimension. The best forecasts are based on plaquettes that extend approximately 1 wavelength downwind and one-half wavelength across-wind.

## V. CONCLUSIONS

### A. Utility and limitations of spatial forecasting

A variety of techniques for forecasting time series can be applied to spatial patterns—subject to the same limitations. Chaotic time series and patterns cannot be conclusively identified by properties of forecasting errors, because nonchaotic systems can mimic one or more of the forecasting signatures of chaotic systems. For example, a sine curve with correlated phase distortion [Fig. 6, as defined in Eq. (3)] has (1) forecasting errors that increase with prediction time (or distance), (2) errors that are minimized using nonlinear models at moderately low dimension, and (3) errors that differ significantly from those of surrogates. Although forecasting cannot be used to distinguish all kinds of dynamics, it is nevertheless a useful technique for evaluating some null hypotheses and for determining what kinds of synthetic or surrogate systems mimic an original.

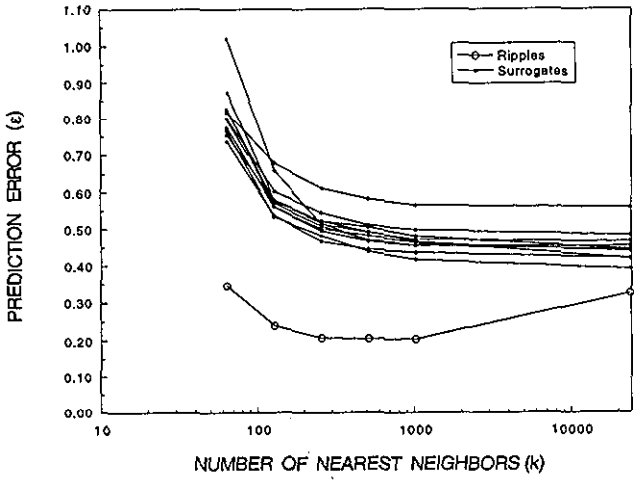


FIG. 15. Forecasting error as a function of number of nearest neighbors for wind ripples and 11 surrogates. Plaquette size is 9 pixels (downwind) by 5 pixels (across-wind), as determined to be optimum in Fig. 14. The best nonlinear model offers a 60% improvement over the best linear model, and the original differs considerably from the surrogates (values of sigma as large as 8).

### B. Natural ripples

The observed dynamic behavior of ripples (downcurrent coupling, sensitivity to initial perturbations, organization into lanes, modification of the near-bed flow and sand-transport field) suggest that complexity of ripple geometry may result from nonperiodic, deterministic, nonlinear interaction between ripples—rather than randomness or quasiperiodicity. This hypothesis is supported by three forecasting properties of the ripples: decaying predictability with forecasting distance, minimized error using nonlinear models at moderate embedding dimension, and significant differences in forecasting properties from surrogate patterns. Ripple geometry is most accurately forecast using sample predictees that extend one wavelength downwind and one-half wavelength across-wind; this result supports the idea that the geometry of any one ripple depends on the geometry of the ripple immediately upstream.

## ACKNOWLEDGMENTS

The author thanks John Sidorowich (University of California San Diego) and James Theiler (Los Alamos National Laboratory) for discussions that improved this paper. Some computational experiments exploring the behavior of periodic and quasiperiodic one-dimensional time series began as wagers with James Theiler. The manuscript was reviewed by Dave Drake and Jim Gardner (U.S. Geological Survey), Jim Crutchfield, and Karl Young (University of California Berkeley), and James Theiler. Part of this work was supported by NASA Grant No. W-17 975.

[1] J. P. Gollub and H. L. Swinney, Phys. Rev. Lett. **35**, 927 (1975).
[2] J. P. Gollub, S. V. Benson, and J. Steinman, Ann. N.Y. Acad. Sci. **357**, 22 (1980).
[3] J. P. Crutchfield, EEE Trans. Circuits and Sys. **35**, 770 (1988).
[4] J. P. Crutchfield and K. Kaneko, "Phenomenology of Spatio–Temporal Chaos," in *Directions in Chaos*, edited by Hao Bai-lin (World Scientific, Singapore, 1987), Vol. 1, pp. 272–353.
[5] A. V. Gaponov-Grekov and M. I. Rabinovich, Physics Today **43**, 30 (1990).
[6] J. P. Crutchfield, "Discovering Coherent Structures in Nonlinear Spatial Systems," Santa Fe Institute publication 91-09-034, p. 26 (1991).
[7] R. E. Livezey and A. G. Barnston, J. Geophys. Res. **93 D9**, 10953 (1988).
[8] J. D. Farmer and J. J. Sidorowich, "Exploiting Chaos to Predict the Future and Reduce Noise," in *Evolution, Learning, and Cognition*, edited by Y. C. Lee (World Scientific, New York, 1989).
[9] G. Sugihara and R. H. May, Nature **344**, 734 (1990).
[10] M. Casdagli, J. R. Stat. Soc. B **54**, 303 (1992).
[11] M. Casdagli, D. Des Jardins, S. Eubank, J. D. Farmer, J. Gibson, N. Hunter, and J. Theiler, "Nonlinear Modeling of Chaotic Time Series: Theory and Applications," in *Applied Chaos*, edited by J. Kim and J. Stringer (Wiley, New York, 1992), pp. 335–380.
[12] J. Theiler, S. Eubank, A. Longtin, B. Galdrikian, and J. D. Farmer, Physica D **58**, 77 (1992).
[13] J. Theiler, P. S. Linsay, and D. M. Rubin, "Detecting Nonlinearity in Data with Long Coherence Times," submitted to Proceedings of the NATO Workshop on Comparative Time Series Analysis, 14–17 May, 1992.



Downloaded 28 Apr 2005 to 192.58.150.41. Redistribution subject to AIP license or copyright, see http://chaos.aip.org/chaos/copyright.jsp

[14] P. Crutchfield and B. S. McNamara, Complex Systems **1**, 417 (1987).
[15] T. P. Meyer, F. C. Richards, and N. H. Packard, Phys. Rev. Lett. **63**, 1735 (1989).
[16] J. P. Crutchfield and K. Young, Phys. Rev. Lett. **63**, 105 (1989).
[17] J. R. L. Allen, Sedimentary Geology **20**, 17 (1978).
[18] D. M. Rubin, *Cross-Bedding, Bedforms, and Paleocurrents* (Society of Economic Paleontologists and Mineralogists, Tulsa, Oklahoma, 1987).
[19] C. Paola and L. Borgman, Sedimentology **38**, 553 (1991).
[20] R. S. Anderson, Earth-Science Reviews **29**, 77 (1990).
[21] S. B. Forrest and P. K. Haff, Science **255**, 1240 (1992).
[22] A. J. Raudkivi, ASCE J. Hydraulics Division **89**, No. 6, 15 (1963).
[23] J. B. Southard and J. R. Dingler, Sedimentology **16**, 251 (1971).
[24] J. R. L. Allen, *Current Ripples; Their Relation to Patterns of Water and Sediment Motion* (North-Holland, Amsterdam, 1968).
[25] G. V. Middleton and J. B. Southard, *Mechanics of Sediment Movement* (Society of Economic Paleontologists and Mineralogists, Tulsa, 1984).



Downloaded 28 Apr 2005 to 192.58.150.41. Redistribution subject to AIP license or copyright, see http://chaos.aip.org/chaos/copyright.jsp